

Switching the Persistent Spin Helix Orientation in Gate-Controlled Double GaAs Quantum Wells

S. Chander^{1,4}, B. W. Grobecker¹, A. V. Poshakinskiy², S. Anghel¹, T. Mano³, J. N. Moore⁴, G. Yusa⁴ and M. Betz¹

¹*Experimentelle Physik 2, Technische Universität Dortmund, Otto-Hahn-Straße 4a, D-44227 Dortmund, Germany*

²*ICFO-Institut de Ciències Fòniques, The Barcelona Institute of Science and Technology, 08860 Castelldefels, Spain*

³*National Institute for Materials Science, Tsukuba, Ibaraki 305-0047, Japan*

⁴*Department of Physics, Tohoku University, Sendai 980-8578, Japan*

E-mail address: markus.betz@tu-dortmund.de, sergiu.anghel@tu-dortmund.de

ABSTRACT. Employing time-resolved Kerr rotation microscopy we demonstrate electrical control over the orientation of the persistent spin helix in a double GaAs quantum well structure equipped with independent front and back gates. We map spin polarization patterns under varying gate voltages and show that coordinated tuning of the two gates enables switching between two orthogonal PSH orientations. This is achieved by inverting the Rashba spin-orbit coupling parameter while maintaining a stable electron density, thus overcoming the leakage-current limitations inherent to single-gate systems. Fourier analysis of the spin maps provides quantitative extraction of spin-orbit coupling strengths, revealing that the Dresselhaus term remains nearly constant while the Rashba parameter is controlled by the difference between the gate voltages. These results establish dual-gate quantum well architectures as an effective platform for precise PSH manipulation and highlight their potential for spintronic applications such as spin-logic devices, long-distance spin interconnects.

KEYWORDS: persistent spin helix, two-dimensional electron gas, time-resolved Kerr rotation, Rashba spin-orbit coupling, Dresselhaus spin-orbit coupling, electron concentration, spin-lifetime, spin diffusion coefficient, back-gate voltage modulation, PSH orthogonal rotation.

I. INTRODUCTION.

The interplay of spin-orbit coupling (SOC) and electron motion in two-dimensional electron gases (2DEGs) has emerged as a central theme in semiconductor spintronics. In particular, the concept of the persistent spin helix (PSH) has attracted significant attention, as it represents a unique regime where spin states are robust against typical spin-dephasing mechanisms. The PSH occurs in (001)-grown zinc-blend structures when Rashba α [1] and Dresselhaus β [2] SOC contributions are balanced, leading to a unidirectional effective spin-orbit field that leads to emergence of spatial spin-density oscillations, either in $[110]$ or $[\bar{1}\bar{1}0]$ direction, depending on the relative sign of α and β , with long coherence distances [3]. Experimental demonstrations in GaAs quantum wells have confirmed the existence of this state, showing spin lifetimes enhanced by up to two orders of magnitude compared with unbalanced systems [4,5]. This has established the PSH as a promising candidate for spin-based information processing and coherent spin transport.

Following its initial realization, numerous studies have focused on the mechanisms that stabilize or limit the

PSH. Experimental and theoretical work has shown that higher-order SOC terms, notably the cubic Dresselhaus contribution, impose fundamental limits on PSH lifetimes, while factors such as carrier density, temperature, and electric fields influence both spin diffusion and relaxation [6-11]. Techniques including gate control of SOC, quantum well orientation and design, and optical doping have enabled tuning of the Rashba-Dresselhaus balance and extending the parameter space where the spin helices can be realized [9,12-14]. Together, these advances highlight both the robustness and fragility of the PSH state, as well as the delicate interplay of structural, electronic, and dynamic factors that govern spin coherence.

Building on this foundation, recent works have explored novel regimes of PSH dynamics. We have demonstrated field-controlled anisotropic spin transport, traveling persistent spin helices under drift, and the influence of carrier density, showing that the longest spin lifetimes do not always coincide exactly with the $|\alpha| = |\beta|$ condition, but also depend on scattering and transport regimes [15-17]. Further studies have extended the concept to quasi-one-dimensional channels [18,19] and two-dimensional grids [20], where lateral confinement restricts the diffusion and slows down the spin relaxation, and to

multiband systems supporting complex spin textures such as skyrmion lattices [21].

The ability to tune simultaneously Rashba and Dresselhaus parameters in double-gated structures was demonstrated via indirect magnetoresistance measurements, where the shape of the weak localization peak was used to detect the PSH state [12, 22]. This approach allowed continuous locking and switching between $|\alpha| = |\beta|$ configurations. However, without the direct imaging of the spin state, the PSH spatial orientation, as well the possibility to control it remained unexplored. In a more recent theoretical study of (110)-oriented GaInAs quantum wells that have two occupied subbands, it has been theoretically shown how to create and control two PSHs simultaneously [23].

In this paper, we use Kerr rotation microscopy to demonstrate a 90-degrees rotation of the PSH in a double (001) GaAs quantum well structure. Such switching is achieved by an inversion of the Rashba parameter, in contrast to its continuous variation as in Ref. [22]. For this, we use the coordinated change of the applied back and front-gate voltages in opposing directions (one increases and the other decreases), thus precisely controlling the electric field across the quantum wells and, consequently, the Rashba parameter, while concurrently maintaining the electron density and avoiding any current leak.

These efforts not only deepen the fundamental understanding of SOC-mediated spin dynamics but also open routes toward practical applications. The demonstrated switching between two long-lived PSH states can be used to enable operation of a spin transistor [23,24]. Moreover, since the states of the transistor feature spin oscillations in orthogonal directions, more complex logical devices can be designed that would enable spin routing in different in-plane directions.

II. EXPERIMENTAL METHODS

The double quantum well (QW) sample was grown in (100) orientation using molecular beam epitaxy. The QWs consist of two 15 nm GaAs layers separated by three monolayers of AlAs and sandwiched between $\text{Al}_{0.24}\text{Ga}_{0.76}\text{As}$ barriers, see Fig. 1(a) (for more details on wafer structure, please see Fig. S1 [25]). Two Si δ -doping layers are placed above, and one below the double quantum well structure, providing a resident electron concentration n in the QWs that can be tuned by the back-gate and front-gate voltage U_{BG} and U_{FG} . The sample is

patterned in a Hall bar geometry (see Fig. 1(b)) with a semi-transparent 14-nm-thick Au front gate, a back gate and AuGeNi ohmic in-plane contacts. To create robust electron spin polarization, the sample resides in a compact cold-finger cryostat, ensuring a lattice temperature of 3.5 K for all performed measurements.

The time-resolved magneto-optical Kerr microscopy (TR-MOKE) measurements are performed using pulses with a temporal width of ~ 35 fs derived from a 60 MHz mode-locked Ti: Sapphire oscillator. Subsequently, they are split into pump and probe paths, which are spectrally tuned independently by grating-based pulse shapers [26]. The resulting pulses have a bandwidth of ~ 0.5 nm and allow for a transform-limited temporal resolution of ~ 1 ps. The probe pulses are linearly polarized while the pump pulses are modulated between left (σ^+) and right (σ^-) circular polarization by an electro-optical modulator (EOM). Both probe and pump pulses are collinearly focused on the sample surface through a 50 \times microscope objective. The full width at half-maximum

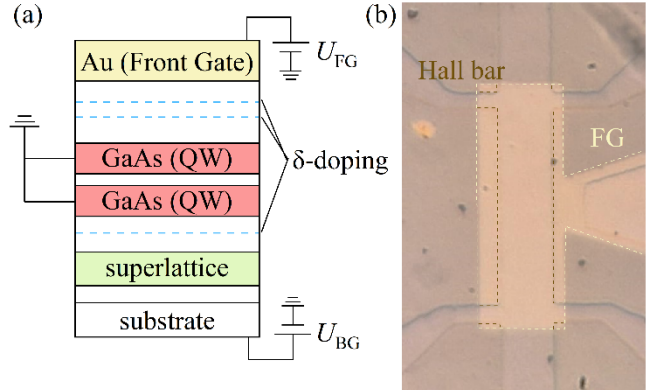


Figure 1. (a) Schematic of the wafer structure. The white layers indicate AlAs barriers and $\text{Al}_{0.24}\text{Ga}_{0.76}\text{As}$. Both quantum wells are contacted and held at ground potential. Independent front-gate (U_{FG}) and back-gate (U_{BG}) voltages can be applied. (b) Device layout featuring a Hall bar geometry. The device is covered by a semitransparent front gate. Brown and yellow lines indicate the mesa and the front gate, respectively.

(FWHM) diameter of pump and probe pulses are $w_0 = 3 \pm 0.1 \mu\text{m}$ and $1 \pm 0.1 \mu\text{m}$ respectively. The reflected pump light is filtered out with a monochromator and the Kerr-rotation of the reflected probe pulse is measured using balanced photodiodes connected to a lock-in amplifier referenced to the EOM frequency. The delay time t between the pump and probe pulses is adjusted by a

mechanical delay stage with $t_{max} = 1.8 \text{ ns}$. The spatial overlap of the pump with the fixed and centered probe is adjusted through a lateral translation of the input lens of a beam-expanding telescope in the pump path [27,28]. In our setup, we scan the position of the pump beam while keeping the probe beam fixed. As a result, the obtained spatial maps can be considered "inverse maps", as they depict spin polarization at a fixed detection point while varying the location where the spin polarization is initially generated. The pump and probe photon energies are chosen

based on the spectral response of the 2DEG, see for example Ref [16].

All measurements are performed with the pump photon energy set to $E_p = 1.57 \text{ eV}$, which is 40 meV above the bandgap energy (1.53 eV), and a peak power density of $I_p = 4.7 \text{ MW/cm}^2$. The probe photon energy is tuned to $E_{pr} = 1.53 \text{ eV}$ with a pulse peak irradiance of $I_{pr} = 2.36 \text{ MW/cm}^2$.

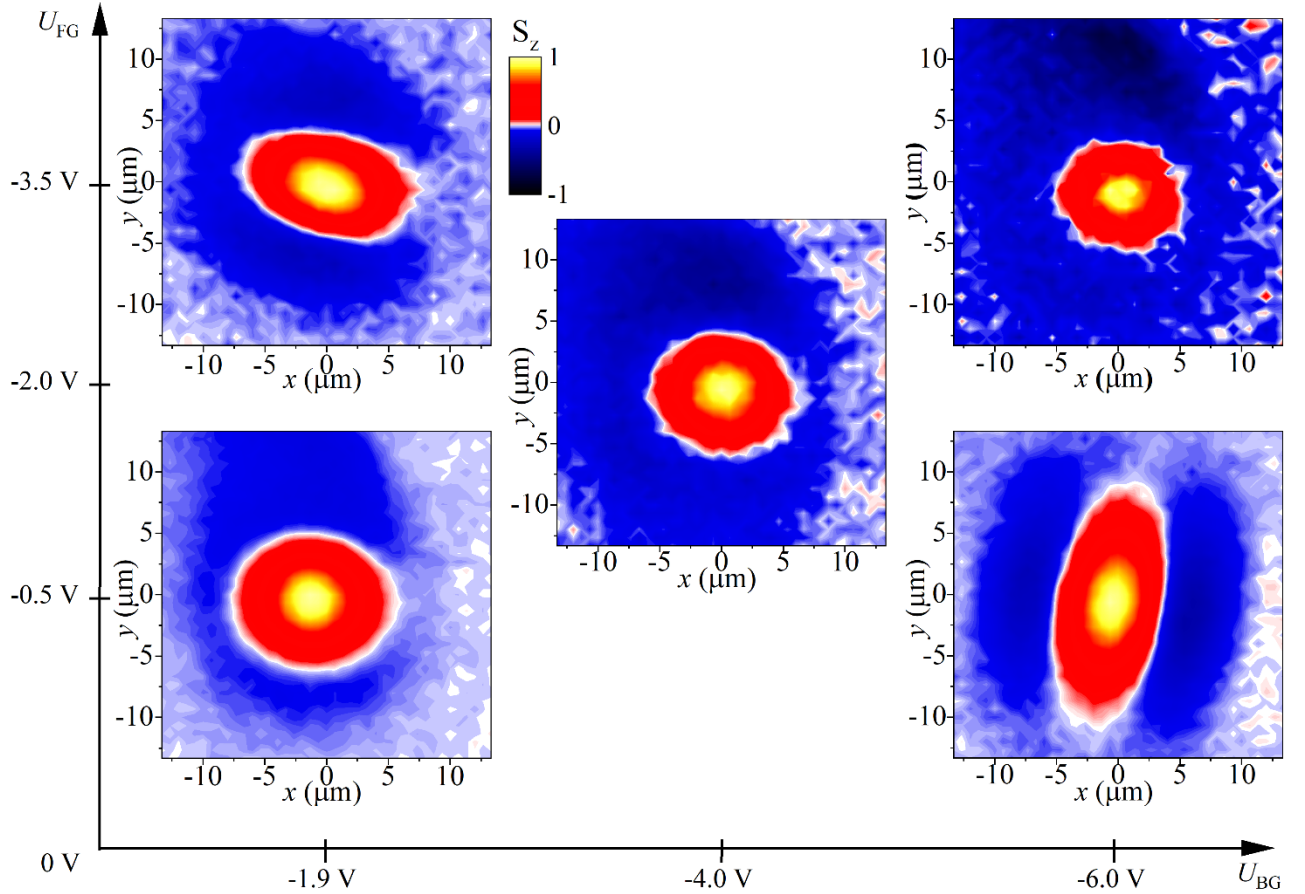


Figure 2. 2D maps of spin polarization, illustrating the manipulation (a 90-degree rotation of the PSH pattern, cf. maps in the top left and the bottom right corners) of the PSH by varying front-gate U_{FG} and back-gate U_{BG} voltages. The delay time for all the measurements was fixed at $t = 500 \text{ ps}$. This figure shows only a representative subset of the full set of measurements, shown in the Supplementary Fig. S2 [25].

III. RESULTS AND DISCUSSION

Figure 2 illustrates the impact of both front and back-gate voltages on the PSH pattern. This figure presents a series of representative 2D PSH maps, each captured at a 500 ps delay time and for the same spatial dimensions, representing various combinations of applied back and front-gate voltages. It is worth noting that this series includes only a few of the many available 2D maps, for the full range see Supplementary Fig. S2 [25]. The back-gate voltage was varied within the range of $0 V < U_{BG} < -6 V$, while the front-gate voltage was adjusted between $0 V < U_{FG} < -3.5 V$. The permissible range for these voltages is determined by the leakage current specific to each case. As evident in Figure 1, different combinations of back and front-gate voltages lead to distinct 2D PSH patterns. A striking observation is the possibility of the 90-degree rotation of the PSH pattern, cf. maps in the top left and the bottom right corners, suggesting that by tuning the back and front-gate voltages in opposite direction one can manipulate the PSH orientation.

The PSH orientation is determined by the relative signs of the Rashba and Dresselhaus parameters. The Dresselhaus parameter typically is not very tunable, as it is set by the bulk inversion asymmetry of the crystal. In contrast, the Rashba parameter is highly controllable. It is governed by the structure inversion asymmetry — specifically, the electric field across the quantum well $\alpha = \gamma_R E_z$ (where γ_R is the Rashba coefficient for GaAs QWs [31])— which can be easily manipulated with a gate voltage. However, in conventional single-gate systems (e.g., a back gate), altering the sign of α would require reversing the gate voltage's polarity. This presents a problem: the voltage range without current leakage is asymmetrical. The negative polarity range is significantly larger than for positive polarity. Since PSH conditions often occur with a negative back-gate voltage, reversing the polarity to achieve the same Rashba value with an opposite sign would require applying a positive gate voltage that exceeds the current leakage threshold and would damage the structure.

The investigated sample, however, effectively addresses this challenge through the coordinated action of its back and front-gates. This configuration facilitates the inversion of the Rashba parameter while concurrently avoiding any current leak, thereby enabling the PSH rotation. This distinctive capability originates from the specific architectural design: the quantum wells are electrically grounded, and the back and front gates (along

with the Si δ -doping layers) are strategically positioned on opposite sides of the QWs, as depicted in Figure 1. The

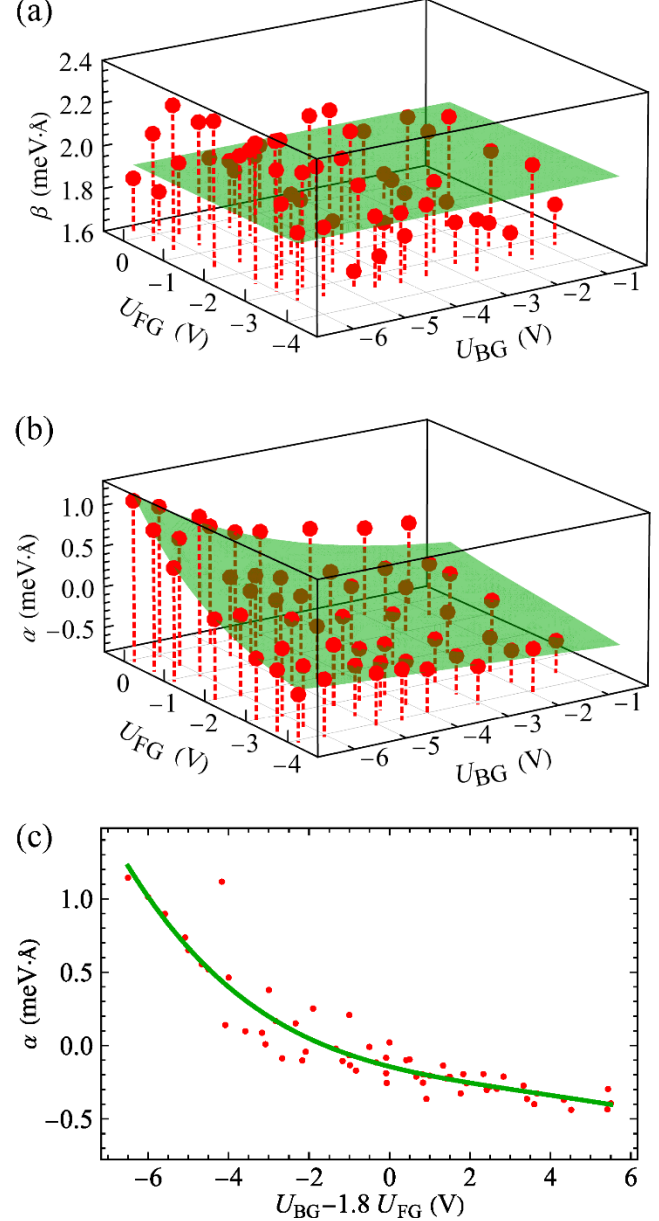


Figure 3. Spin-orbit interaction parameters extracted from the 2D spin polarization maps, by fitting to Eq. 1 (after applying the fast Fourier transformations): (a) Dresselhaus parameter β and (b) Rashba parameter α as functions of front-gate (U_{FG}) and back-gate (U_{BG}) voltages. A green plane in both plots indicates a fit to the extracted data. (c) Rashba parameter α plotted against the combined gate voltage term $U_{BG} - 1.8 U_{FG}$, based on the fit in (b).

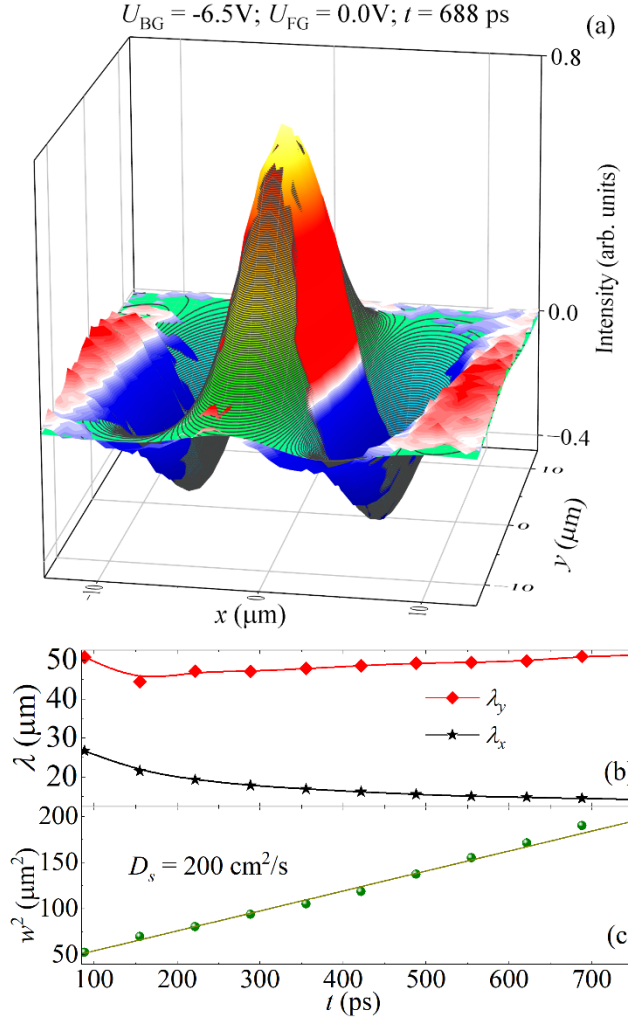


Figure 4. (a) The fit of the 2D spin polarization map for gate voltage combination: $U_{BG} = -6.5\text{ V}$, $U_{FG} = 0.0\text{ V}$, and a delay time of $t = 688\text{ ps}$. The surface colored by red and blue represents experimental data; green surface is the fit after Eq. (2). (b, c) Temporal evolution of the spin precession lengths $\lambda_x(t)$, $\lambda_y(t)$, and the squared FWHM $w^2(t)$ (together with a linear fit to extract the diffusion coefficient), extracted from the fit set.

choice of a double quantum well structure was not critical to this experiment, and we expect that a single quantum well structure would yield the same qualitative results.

By adjusting the front and back-gate voltages in the same direction (both either increase or decrease), one can uniformly lower or raise the energy bands thus controlling the electron density in the QWs. Conversely, by adjusting the gate voltages in opposing directions (one increases and the

other decreases), one precisely controls the electric field (including flipping its sign) across the quantum well and, consequently, the Rashba parameter. This latter mode of differential tuning is precisely what is required to switch the PSH direction while preserving the optimal electron density indispensable for PSH formation. This specific tuning corresponds to the trajectory between the top-left and bottom-right corners of Figure 2. In sharp contrast, tuning of the gate voltages in the same direction, i.e., between the left bottom and right top corners of Fig. 2, leaves the spin maps almost unaffected. The almost round shape of the spin pattern observed in this case indicates an almost isotropic spin-orbit splitting, which corresponds to $\alpha \approx 0\text{ meV} \cdot \text{\AA}$.

To quantify the effect of the back and front-gate voltages on the PSH pattern, it is necessary to extract spin-orbit parameters from each individual measured spin map. For that, fast Fourier transformations are applied along both spatial coordinates and obtained spectra are analyzed, see Supplementary Fig. S3 [25]. The spectra reveal a pair of peaks, corresponding to the wavevectors of the spatial spin oscillations. We fit the spectra with the analytical expression, that follows from the spin-diffusion equation [29]:

$$S_z(k_x, k_y) \propto \exp\left(-\frac{k^2 w_0^2}{16} \ln 2\right) \times \exp\left(-D_s t \begin{bmatrix} k^2 + q_x^2 & 0 & -2ik_x q_x \\ 0 & k^2 + q_y^2 & -2ik_y q_y \\ 2ik_x q_x & 2ik_y q_y & k^2 + q_x^2 + q_y^2 \end{bmatrix}_{zz}\right), \quad (1)$$

where $q_{y(x)} = 2m^*(\beta \pm \alpha)/\hbar^2$ are the spin-precession wave vectors and w_0 is the FWHM of the initial spin distribution. Given that the sample hosts two subbands, and that recent studies have shown that inter-subband interactions in such systems can range from weak to strong ([21,23,31]), the applicability of Eq. (1) is not immediately evident. However, for the high back-gate voltages employed here (up to 6 V) and the relatively small sample thickness ($\sim 1\text{ }\mu\text{m}$), the resulting energetic separation between the subbands at the operating voltages is sufficiently large to render their mutual interaction weak, thereby justifying the use of Eq. (1). Additionally, the fact that the actual crystallographic axes might be slightly misaligned with the axes used in the experiment is also taken into consideration. From the fits the $q_{y(x)}$ parameters are extracted and the spin orbit parameters α and β are calculated.

The intricate effect of back and front-gate voltages on the spin-orbit coupling parameters is revealed in Figs. 3(a) and 3(b). Figure 3(a) demonstrates that the Dresselhaus parameter β is almost invariant across the applied voltage range, as indicated by the green plane which represents the

fit to the extracted data by a constant function, resulting in a value of $\beta = 1.95 \pm 0.15 \text{ meV} \cdot \text{\AA}$. This stability implies a negligible variation on β_3 (the density dependent contribution to β), explained by the fact that photoelectrons significantly enhance the electron density above the magnitude of density change that is achievable by the gate voltage. [16]. Conversely, the Rashba parameter α , depicted in Figure 3(b), shows a pronounced dependence on the gate voltages. A particularly significant finding is the reversal of the Rashba parameter sign when front and back-gate voltages are tuned in opposite directions. This sign change, in conjunction with the preserved value of β , is precisely what enables the electrical switching of the PSH orientation. The fitting suggests that the value of Rashba parameter α is determined by the linear combination of the voltages $U_{BG}-1.8U_{FG}$, which is therefore attributed to controlling the electric field inside the quantum wells. The cross-section along this direction is shown in Fig. 3(c). In the orthogonal direction, i.e., when changing $1.8U_{BG}+U_{FG}$, the Rashba parameter remains consistently constant. This suggests that for the latter voltage combination, the electric fields induced by the back and front gates effectively counteract each other, leading to a stable Rashba parameter. This implies that the electron densities in the front and back quantum wells are respectively $n_f=1.8U_{FG}c_b/e+n_0$ and $n_b=U_{BG}c_b/e+n_0$, where c_b is the capacitance per unit area of the back gate with the 2DEG, and n_0 is the electron density contributed by doping and optical excitation. This also implies that the field effect from the front gate is 1.8 times stronger than the back gate, though the relative difference expected from the dielectric layer thicknesses is actually about 6. The reduction to 1.8 may be due to partial screening of the front gate by a parallel conducting layer which is populated by electrons photoexcited out of the doping layers [32].

While the theory predicts that the shape of the spin distribution in the reciprocal space is described by quite simple analytical Eq. (1), there is no exact analytical expression for the real-space distribution. Instead, to describe the real-space distribution we propose using an approximate empirical formula:

$$S_z(x,y)=A e^{-\frac{4 \ln(2)(x^2+y^2)}{w^2}} \cos 2\pi \sqrt{\left(\frac{x}{\lambda_x}\right)^2 + \left(\frac{y}{\lambda_y}\right)^2}, \quad (2)$$

where w is the FWHM of the distribution and $\lambda_{x(y)}$ are the spin precession lengths along the $x(y)$ direction. As previously, we additionally take into account small axes rotation, to account for misalignment with the

crystallographic axes. As an example, we show in Fig. 4 the fit results for the voltages $U_{BG}=-6.5 \text{ V}$, $U_{FG}=0.0 \text{ V}$ and a delay time of $t=688 \text{ ps}$. Fig. 4(a) demonstrates a very good agreement between the fit and the original data, particularly regarding the signal shape and the oscillating spin pattern.

Subsequently, we fit the spatial 2D maps (for the above mentioned combination of the back- and front-gate voltages) of spin distribution at different moments of time with Eq. (2) and extract the temporal dependence of the amplitude $A(t)$, FWHM $w(t)$, and the spin-precession lengths $\lambda_{x(y)}(t)$ (for all the 2D maps used for this fit, please see the Fig. S4 [25]). The temporal dependence of the extracted spin precession lengths is shown in Fig. 4(b). It is worth noting that $\lambda_x(t)$ and $\lambda_y(t)$ depend on time in quite distinct ways. First, they both start at some larger values and for a short period of time $t \lesssim 150 \text{ ps}$, both decrease, indicating the formation of the spin-density oscillations along both x and y directions, which originate from the spin precession in the spin-orbit fields acting on electrons moving in the corresponding direction. For longer delay times, all the spin modes get suppressed, except for the most long-living mode, which is the PSH mode with oscillations along x direction only for the chosen voltages. In contrast, $\lambda_y(t)$ reaches a minimum (determined by the interplay of w_0 and the spin-orbit parameters) and then starts to grow again, indicating that the spin oscillations along y direction disappear at larger delay times, as it is expected for the direction orthogonal to the PSH mode. The limiting value of $\lambda_x(t)$ at $t \rightarrow \infty$ allows to calculate the combination of the spin-orbit parameters $|\alpha|+|\beta|=\pi\hbar^2/m^*\lambda_x(\infty) \approx 2.8 \text{ meV} \cdot \text{\AA}$. However, the value of $|\alpha|-|\beta|$ cannot be extracted in a simple way from the $\lambda_y(t)$ dependence. We also analyze the FWHM temporal dependence $w(t)$, Fig. 4(c). We fit it with a linear function and determine the spin diffusion coefficient $D_s=200 \pm 10 \text{ cm}^2/\text{s}$ from its slope. Finally, we also fit the temporal dependence of the spin volume $A(t) \cdot w^2(t)$ with an exponential function (not shown), to determine the spin lifetime.

Figure 5 presents the extracted spin-diffusion coefficient and spin lifetime as a function of the back and front-gate voltages. It is immediately apparent that both parameters are not constant across the voltage range combination and exhibit an inverse trend, which is consistent with the relationship $T_s \propto 1/D_s$ [15]. The variation of the spin diffusion coefficient with the gate voltages, despite the relatively constant electron concentration (see the discussion around Fig. 3(a)), can be attributed to the change of the

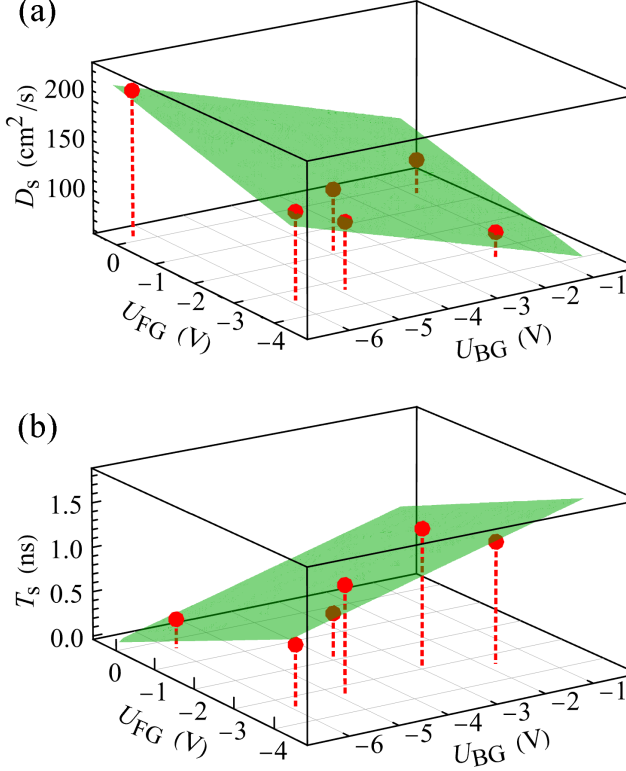


Figure 5. Extracted (a) spin diffusion coefficient D_s and (b) spin lifetime T_s as functions of front-gate (U_{FG}) and back-gate (U_{BG}) voltages, showing that both parameters are not constant across the voltage range combination and exhibit an inverse trend. The green plane in each plot represents the best fit to the data.

electron scattering time τ_p^* caused by the gate voltage pushing electrons towards certain QW interfaces [19].

IV. CONCLUSIONS

This study demonstrates a novel approach for manipulating the persistent spin helix pattern by employing a dual-gate GaAs double quantum well structure. Using independent front and back gates, we achieved fine control of spin-orbit interactions and showed that the PSH orientation can be between the two crystallographic directions. This was realized by inverting the Rashba spin-orbit coupling parameter while keeping the Dresselhaus parameter and carrier density nearly constant, overcoming leakage-current limitations of conventional single-gate designs. Time-resolved Kerr rotation microscopy, combined with Fourier analysis of spin polarization maps, enabled us

to directly visualize the reorientation process and quantitatively extract the gate dependence of Rashba and Dresselhaus terms. Our results reveal that while the Dresselhaus contribution remains essentially fixed, the Rashba coupling exhibits strong tunability under dual-gate operation, providing the key mechanism for PSH direction switching.

These findings establish a versatile platform for precise spin-orbit engineering in two-dimensional electron systems. Beyond demonstrating PSH orientation control, dual-gate design overcomes limitations of single-gate architectures and opens pathways for spintronic devices where robust, reconfigurable spin textures, that enable spin routing in different in-plane directions, are required. Such control is particularly promising for spin logic operations, coherent spin interconnects, and future quantum information technologies that rely on stable and tunable spin states.

ACKNOWLEDGMENTS

A.V.P. acknowledges the funding from the postdoctoral fellowship Beatriu de Pinós (2023 BP 00136), Government of Spain, under Severo Ochoa Grant No. CEX2019-000910-S (MCIN/AEI/10.13039/501100011033), Generalitat de Catalunya (CERCA program), Fundació Cellex, and Fundació Mir-Puig. This work is supported by a Grant-in-Aid for Scientific Research (Grants No. 19H05603, No. 21H05182, No. 21H05188, and No. 24H00399) from the Ministry of Education, Culture, Sports, Science, and Technology (MEXT), Japan.

-
- [1] E. I. Rashba, Properties of semiconductors with an extremum loop. 1. Cyclotron and combinational resonance in a magnetic field perpendicular to the plane of the loop., *Sov. Phys. Solid State* **2**, 1109 (1960).
- [2] G. Dresselhaus, Spin-Orbit Coupling Effects in Zinc Blende Structures, *Physical Review* **100**, 580 (1955).
- [3] B. A. Bernevig, J. Orenstein and S. C. Zhang, Exact SU(2) symmetry and persistent spin helix in a spin-orbit coupled system, *Phys Rev Lett* **97**, 236601 (2006).
- [4] C. P. Weber, J. Orenstein, B. A. Bernevig, S. C. Zhang, J. Stephens and D. D. Awschalom, Nondiffusive spin dynamics in a two-dimensional electron gas, *Phys Rev Lett* **98**, 076604 (2007).
- [5] J. D. Koralek, C. P. Weber, J. Orenstein, B. A. Bernevig, S.-C. Zhang, S. Mack and D. D. Awschalom, Emergence of the persistent spin helix in semiconductor quantum wells, *Nature* **458**, 610 (2009).
- [6] D. Iizasa, D. Sato, K. Morita, J. Nitta and M. Kohda, Robustness of a persistent spin helix against a cubic Dresselhaus field in (001) and (110) oriented two-dimensional electron gases, *Physical Review B* **98** (2018).
- [7] E. Cruz, C. López-Bastidas and J. A. Maytorena, Effect of cubic Dresselhaus interaction on the longitudinal optical conductivity of a spin-orbit coupled system, *Journal of Applied Physics* **123**, 113902 (2018).
- [8] Y. Kunihashi, H. Sanada, Y. Tanaka, H. Gotoh, K. Onomitsu, K. Nakagawara, M. Kohda, J. Nitta and T. Sogawa, Drift-Induced Enhancement of Cubic Dresselhaus Spin-Orbit Interaction in a Two-Dimensional Electron Gas, *Physical Review Letters* **119**, 187703 (2017).
- [9] P. Altmann, F. G. Hernandez, G. J. Ferreira, M. Kohda, C. Reichl, W. Wegscheider and G. Salis, Current-Controlled Spin Precession of Quasistationary Electrons in a Cubic Spin-Orbit Field, *Phys Rev Lett* **116**, 196802 (2016).
- [10] R. Kurosawa, K. Morita, M. Kohda and Y. Ishitani, Effect of cubic Dresselhaus spin-orbit interaction in a persistent spin helix state including phonon scattering in semiconductor quantum wells, *Applied Physics Letters* **107**, 182103 (2015).
- [11] M. Studer, M. P. Walser, S. Baer, H. Rusterholz, S. Schön, D. Schuh, W. Wegscheider, K. Ensslin and G. Salis, Role of linear and cubic terms for drift-induced Dresselhaus spin-orbit splitting in a two-dimensional electron gas, *Physical Review B* **82** (2010).
- [12] K. Yoshizumi, A. Sasaki, M. Kohda and J. Nitta, Gate-controlled switching between persistent and inverse persistent spin helix states, *Applied Physics Letters* **108**, 132402 (2016).
- [13] M. Luengo-Kovac, F. C. D. Moraes, G. J. Ferreira, A. S. L. Ribeiro, G. M. Gusev, A. K. Bakarov, V. Sih and F. G. G. Hernandez, Gate control of the spin mobility through the modification of the spin-orbit interaction in two-dimensional systems, *Physical Review B* **95**, 6, 245315 (2017).
- [14] G. Wang, B. L. Liu, A. Balocchi, P. Renucci, C. R. Zhu, T. Amand, C. Fontaine and X. Marie, Gate control of the electron spin-diffusion length in semiconductor quantum wells, *Nat. Commun.* **4**, 2372 (2013).
- [15] S. Anghel, A. V. Poshakinskiy, K. Schiller, G. Yusa, T. Mano, T. Noda and M. Betz, Spin helices in GaAs quantum wells: Interplay of electron density, spin diffusion, and spin lifetime, *Journal of Applied Physics* **132**, 054301 (2022).
- [16] S. Anghel, A. V. Poshakinskiy, K. Schiller, F. Passmann, C. Ruppert, S. A. Tarasenko, G. Yusa, T. Mano, T. Noda and M. Betz, Anisotropic expansion of drifting spin helices in GaAs quantum wells, *Physical Review B* **103** (2021).
- [17] S. Anghel, F. Passmann, K. J. Schiller, J. N. Moore, G. Yusa, T. Mano, T. Noda, M. Betz and A. D. Bristow, Spin-locked transport in a two-dimensional electron gas, *Physical Review B* **101** (2020).
- [18] P. Altmann, M. Kohda, C. Reichl, W. Wegscheider and G. Salis, Transition of a two-dimensional spin mode to a helical state by lateral confinement, *Physical Review B* **92**, 235304 (2015).
- [19] B. W. Grobecker, A. V. Poshakinskiy, S. Anghel, T. Mano, G. Yusa and M. Betz, Enhancing spin diffusion in GaAs quantum wells: The role of electron density and channel width, *Journal of Applied Physics* **137** (2025).
- [20] A. V. Poshakinskiy, Persistent Spin Grids with a Spin-Orbit-Coupled 2D Electron Gas, *Phys Rev Lett* **135**, 066205 (2025).
- [21] J. Fu, P. H. Penteado, M. O. Hachiya, D. Loss and J. C. Egues, Persistent Skyrmion Lattice of Noninteracting Electrons with Spin-Orbit Coupling, *Phys Rev Lett* **117**, 226401 (2016).
- [22] F. Dettwiler, J. Y. Fu, S. Mack, P. J. Weigle, J. C. Egues, D. D. Awschalom and D. M. Zumbuhl, Stretchable Persistent Spin Helices in GaAs Quantum Wells, *Physical Review X* **7**, 031010 (2017).
- [23] N. Zhao, Y. Duan, H. Yang, X. Li, W. Liu, J. Zhao, S. Han, K. Shen, N. Hao, J. Fu *et al.*, Two copies of spin helices with stretching pitch and compensating helicity, *Physical Review B* **107**, 205407 (2023).

- [24] S. Datta and B. Das, Electronic analog of the electro-optic modulator, *Applied Physics Letters* **56**, 665 (1990).
- [25] See Supplemental Material at [\[url\]](#) for supplementary details about the wafer structure, additional experimental data and fitting procedure.
- [26] S. Anghel, A. Singh, F. Passmann, H. Iwata, J. N. Moore, G. Yusa, X. Li and M. Betz, Enhanced spin-polarization lifetimes in a two-dimensional electron gas in a gate-controlled GaAs quantum well, *Physical Review B* **94**, 035303 (2016).
- [27] T. Henn, T. Kießling, L. W. Molenkamp, D. Reuter, A. D. Wieck, K. Biermann, P. V. Santos and W. Ossau, Time and spatially resolved electron spin detection in semiconductor heterostructures by magneto-optical Kerr microscopy, *physica status solidi (b)* **251**, 1839 (2014).
- [28] T. Henn, T. Kiessling, W. Ossau, L. W. Molenkamp, K. Biermann and P. V. Santos, Ultrafast supercontinuum fiber-laser based pump-probe scanning magneto-optical Kerr effect microscope for the investigation of electron spin dynamics in semiconductors at cryogenic temperatures with picosecond time and micrometer spatial resolution, *Rev. Sci. Instrum.* **84**, 123903 (2013).
- [29] R. Winkler, *Spin-orbit coupling effects in two-dimensional electron and hole systems* (Springer, Berlin ; New York, 2003), Springer tracts in modern physics, 191.
- [30] F. Passmann, S. Anghel, C. Ruppert, A. Bristow, A. Poshakinskiy, S. A. Tarasenko and M. Betz, Dynamical Formation and active control of persistent spin helices in III-V and II-VI quantum wells, *Semiconductor Science and Technology* **34**, 093002 (2019).
- [31] I. R. de Assis, R. Raimondi and G. J. Ferreira, Spin drift-diffusion for two-subband quantum wells, *Physical Review B* **103** (2021).
- [31] M. Reed, W. Kirk and P. Kobiela, Investigation of parallel conduction in GaAs/Al_xGa_{1-x}As modulation-doped structures in the quantum limit, *IEEE Journal of Quantum Electronics* **22**, 1753 (1986).